

# Phase-shifting coronagraph

François Hénault, Alexis Carlotti, Christophe Vérinaud

Institut de Planétologie et d'Astrophysique de Grenoble  
Université Grenoble-Alpes  
Centre National de la Recherche Scientifique  
BP 53, 38041 Grenoble – France

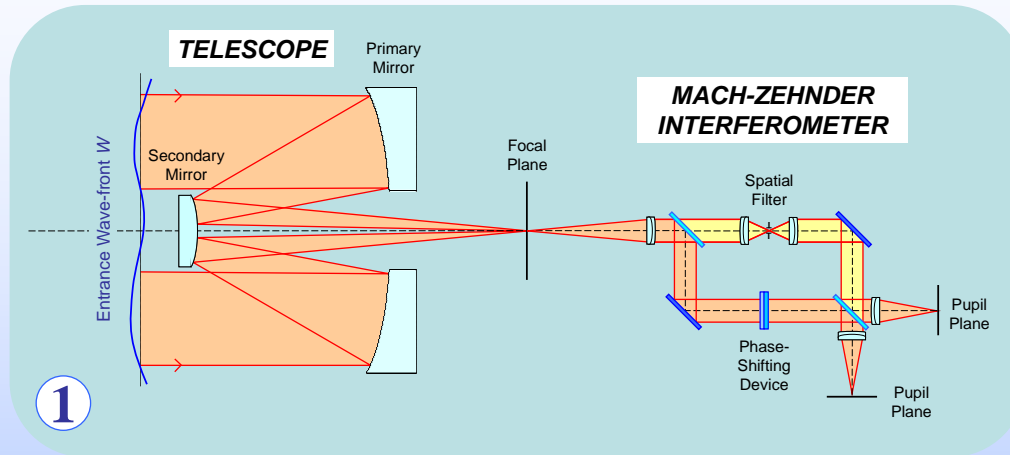
# Plan of presentation

- Goal of the study
- Principle
- Optical design
- Numerical model
  - Simulation of measures intensities
  - Wavefront reconstruction procedure
- Numerical simulations
  - Three different phase-shifting schemes
  - Three types of phase mask coronagraphs
  - Two typical wavefront errors (to be measured)
- Interpretation of the results
- Conclusion

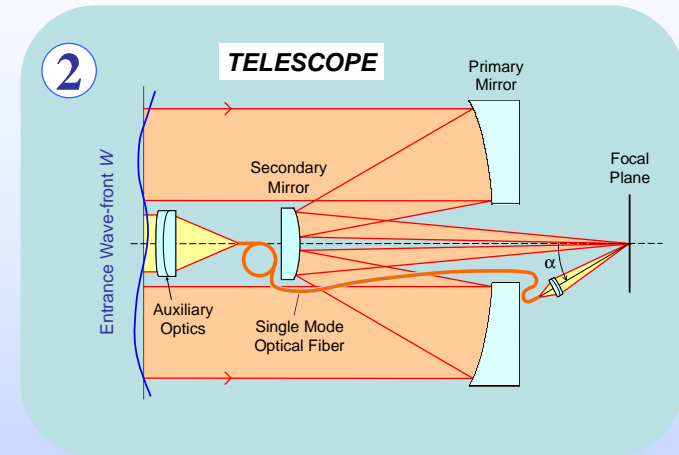
# Goal of the study

- Evaluate the measurement accuracy of wavefront sensing phase-shifting methods **from inside a coronagraph**
- Put the phase-shifting device as far as possible within the coronagraph to compensate for Non common path aberrations (NCPA)
- Compare phase-shifting in the pupil plane with phase-shifting in the image plane
- Evaluate validity range:
  - Limited to weak aberrations or only by  $2\pi$ -ambiguity  $[-\lambda/2, +\lambda/2]$  ?
  - Real or low-order wavefront sensor ?

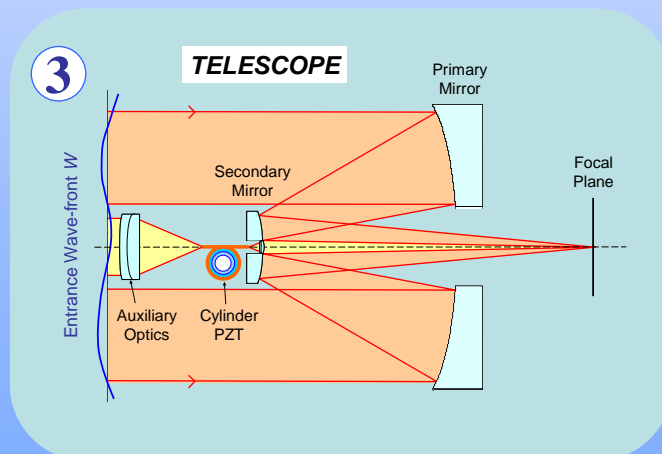
# A brief history of phase-shifting telescopes



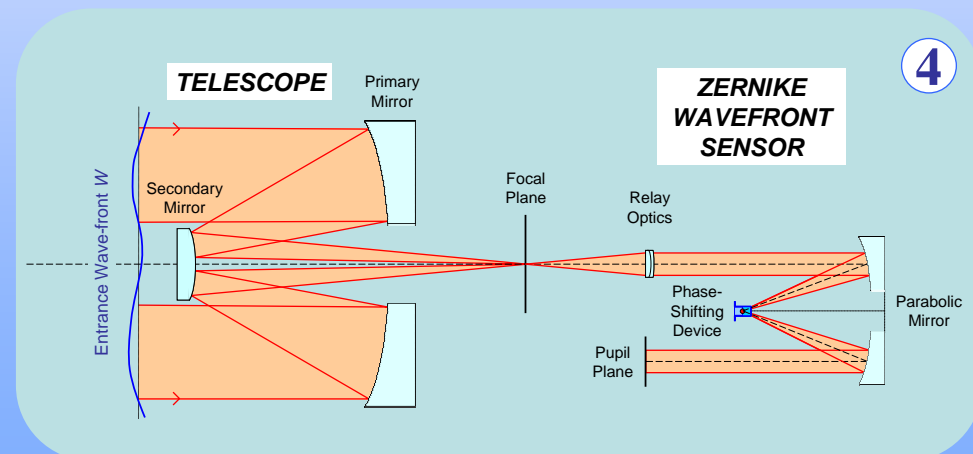
R. Angel, Nature (1994)



F. Hénault, Applied Optics (2005)



F. Hénault, Optics Communications (2006)



J. K. Wallace et al, Proc. SPIE (2011)

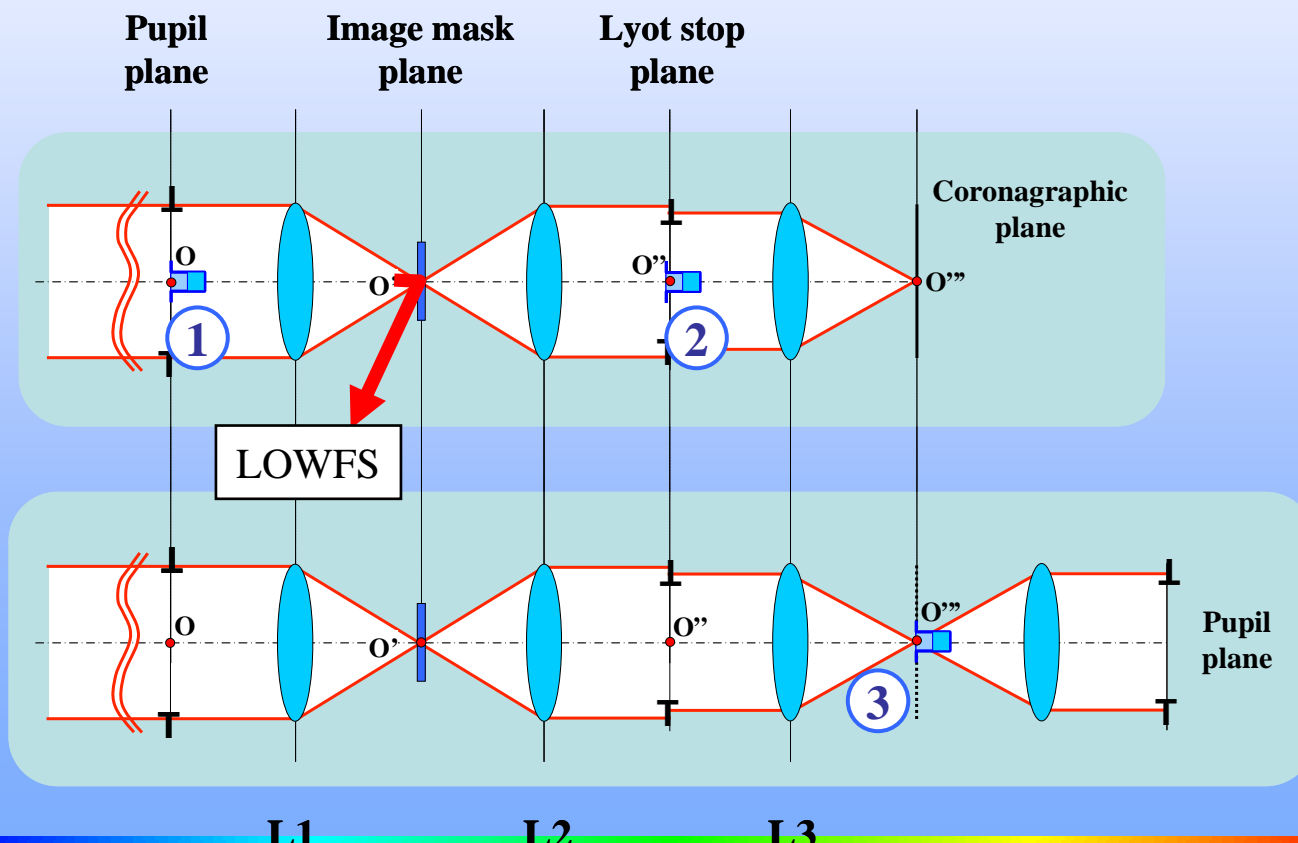
# Principle

- Three different phase-shifting schemes:

Phase-shifting  
device

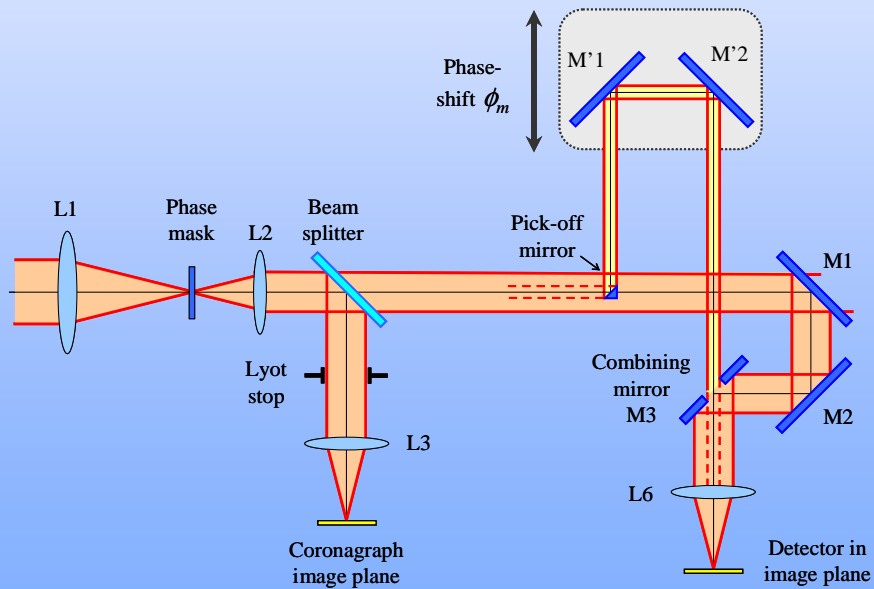


- 1 - In telescope pupil plane
- 2 - In Lyot stop plane
- 3 - In coronagraph image plane

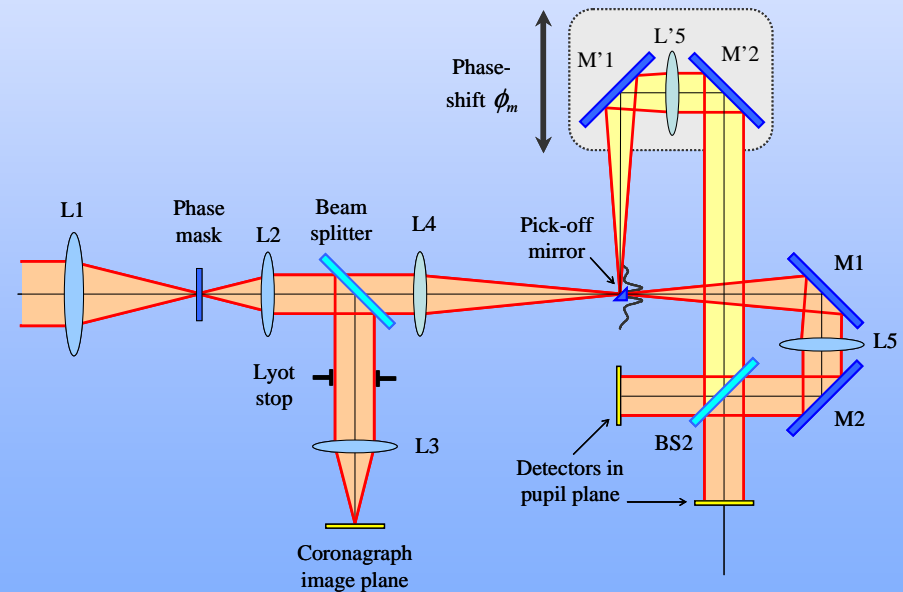


# Optical design

Phase-shifting in  
**Pupil**/Lyot stop plane  
→ Sensing in **image** plane

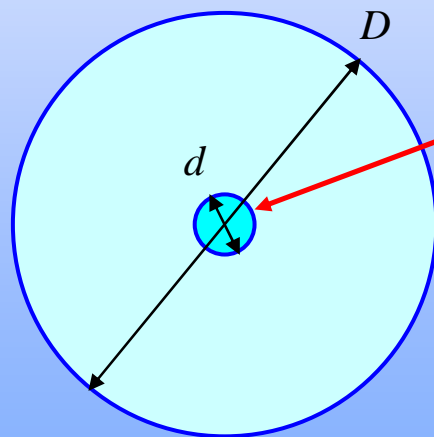


Phase-shifting in  
coronagraph **image** plane  
→ Sensing in **pupil** plane



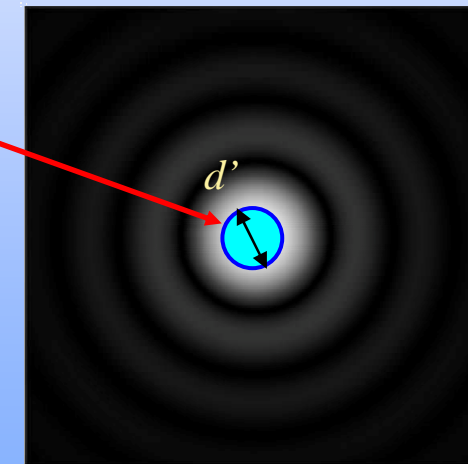
# Numerical model

- **Module 1:** Complex amplitude propagation from plane to plane via Fourier transforms (see next slides)
- **Module 2:** Simplified WFE reconstruction procedure using two Dirac “Delta” approximations



**Delta approximation**  
in **pupil plane**  $d / D \ll 1$

**Phase-  
shifting  
area**

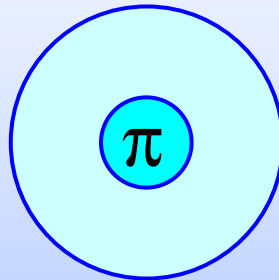


**Delta approximation**  
in **image plane**  $d' < \lambda F/D$

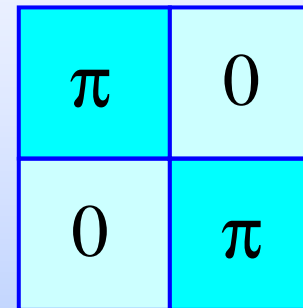
# Numerical simulations

- Three different types of phase mask coronagraphs

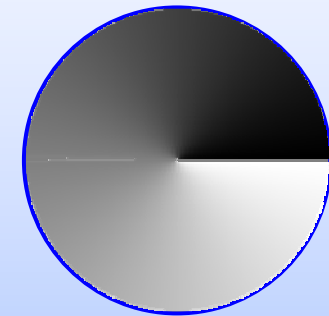
Roddier



Four-  
Quadrant

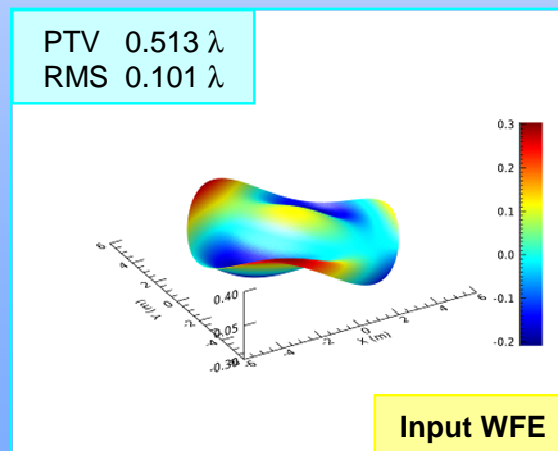


Vortex

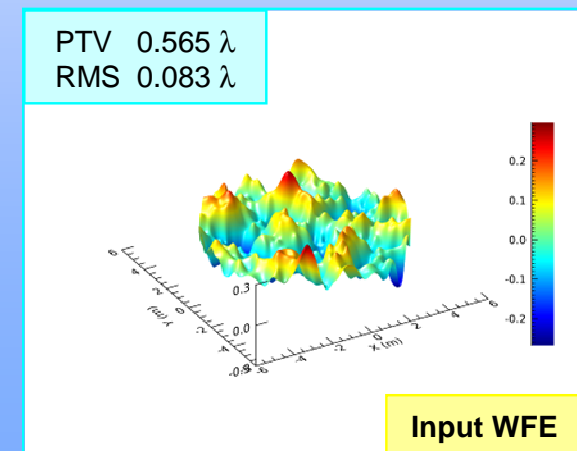


- Two typical wavefront errors

Low spatial  
frequency  
WFE



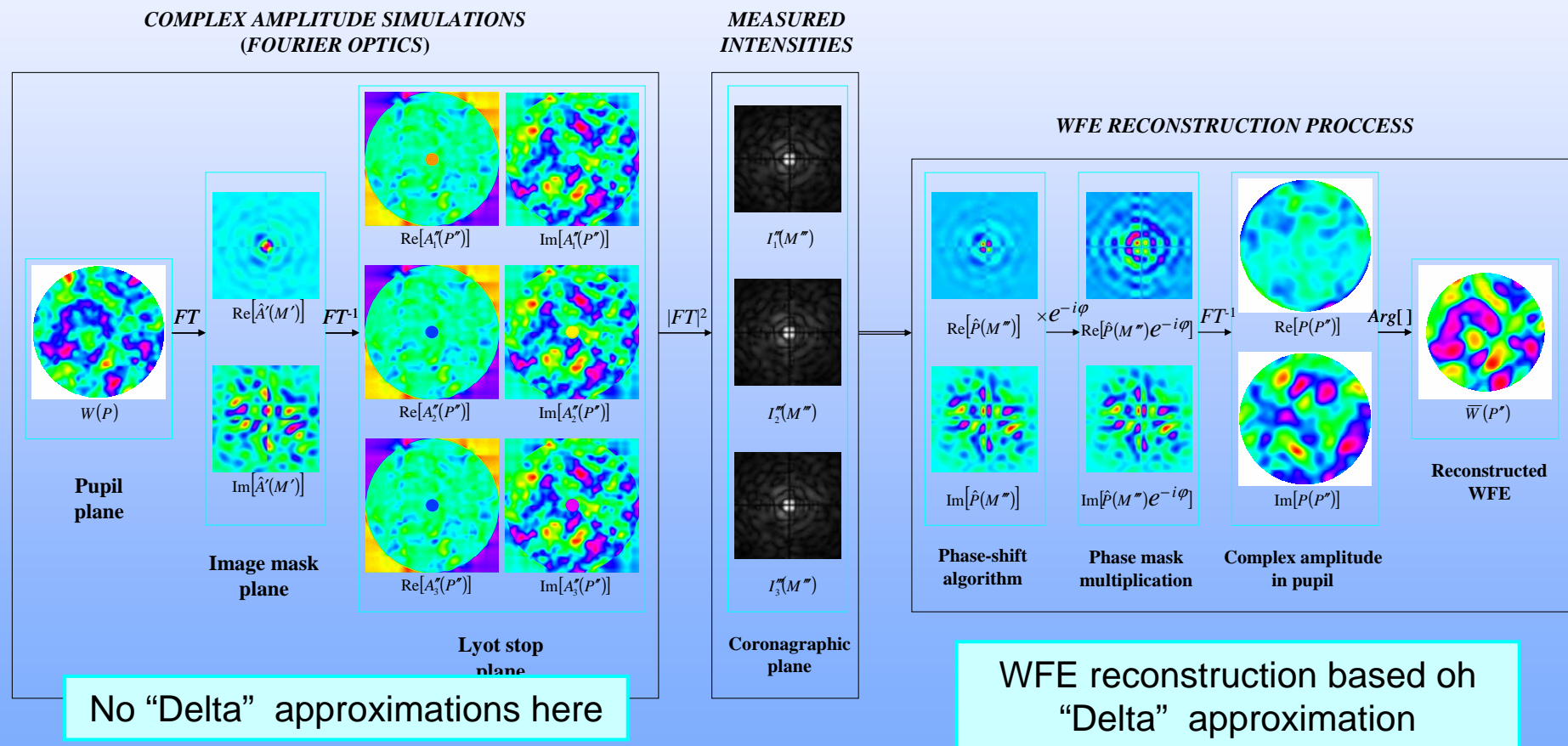
Mid spatial  
frequency  
WFE





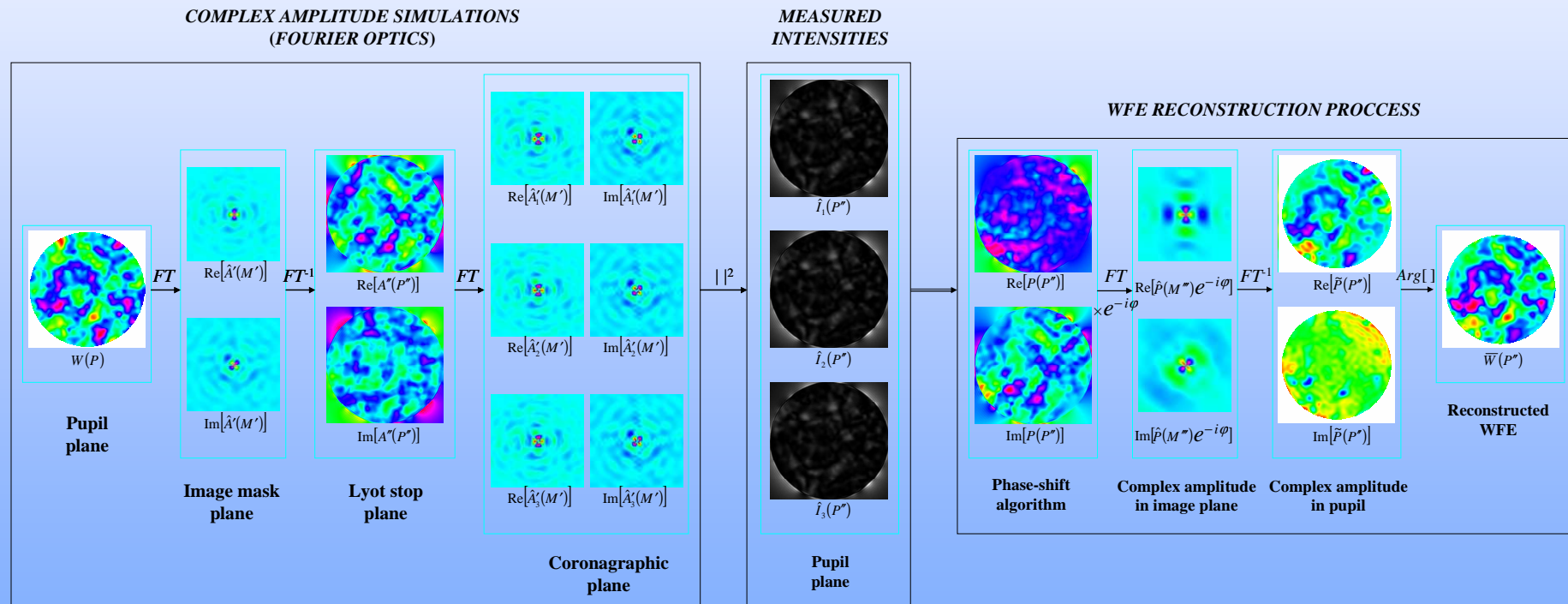
# Numerical simulations

- Phase-shifting in Lyot stop plane (four-quadrant phase mask)



# Numerical simulations

- Phase-shifting in coronagraph image plane (vortex phase mask)



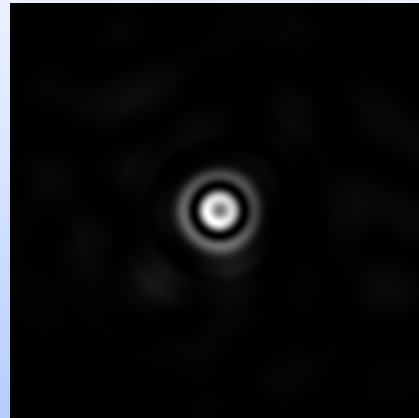
# Measured intensities – 3 sequential phase-shifts

$$\phi_m = 0, 2\pi/3 \text{ and } 4\pi/3$$

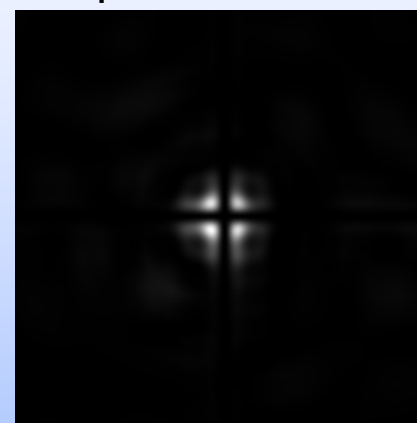
- Phase-shifting in pupil plane
- Sensing in image plane

- Phase-shifting in image plane
- Sensing in pupil plane

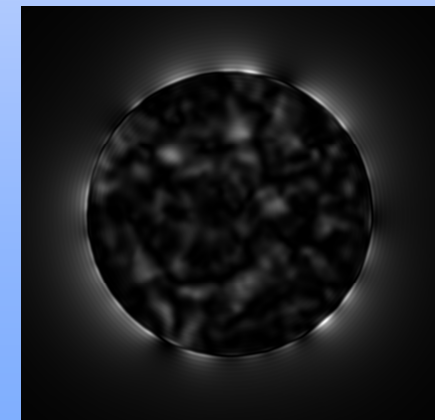
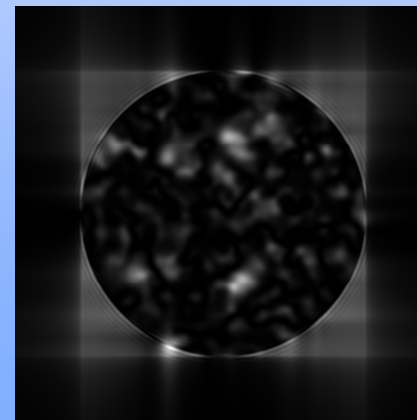
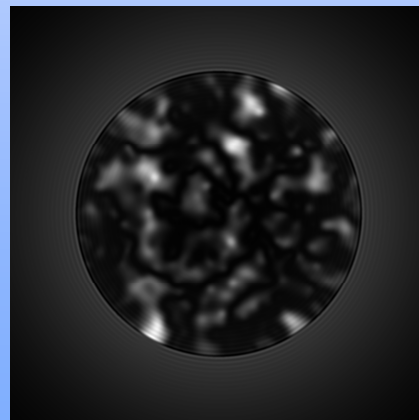
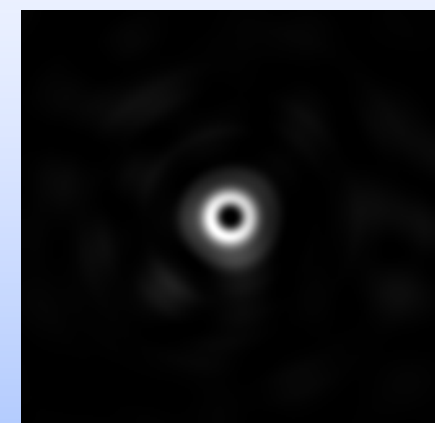
Behind Roddier phase mask



Behind 4-quadrants phase mask



Behind Vortex phase mask



# Numerical results

- Measurement accuracy is fairly **similar for all cases**
  - Low spatial frequency WFE: Typically in the range **5-10 %** well below  **$\lambda/100$  RMS**
  - Mid spatial frequency is slightly worse: 10-15 %
  - As good as when there is no phase mask, except for the four-quadrant

Initial WFE

PTV  $0.513 \lambda$

RMS  $0.101 \lambda$

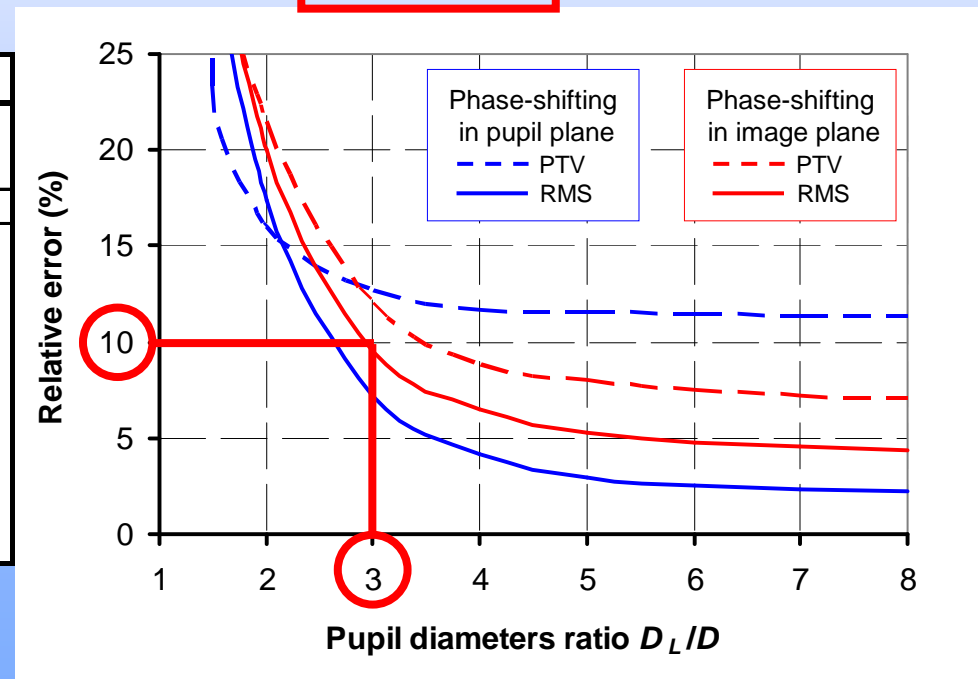
## PHASE-SHIFT LOCATION

| Type of Coronagraph | Telescope pupil plane<br>$\rho = 0.05; \Lambda = 4; 0.1 < \eta < 0.9$ |                    |                    | Lyot stop plane<br>$\rho = 0.05; \Lambda = 4; 0.1 < \eta < 0.9$ |                    |                    | Image plane<br>$\varepsilon = 0.1^{(*)}; \Lambda = 4; 0 < \eta < 0.95$ |                    |                    |     |
|---------------------|---|--------------------|--------------------|---|--------------------|--------------------|--|--------------------|--------------------|-----|
|                     | Measured (waves)  | Difference (waves) | Relative error (%) | Measured (waves)  | Difference (waves) | Relative error (%) | Measured (waves)   | Difference (waves) | Relative error (%) |     |
| No coronagraph      | 0.098   | 0.005              | 5                  | 0.098   | 0.005              | 5                  | 0.106  | 0.002              | 2                  | RMS |
|                     | 0.489   | 0.037              | 7                  | 0.489   | 0.036              | 7                  | 0.516  | 0.017              | 3                  | PTV |
| Roddier             | 0.107   | 0.008              | 8                  | 0.110   | 0.009              | 9                  | 0.104  | 0.007              | 6                  | RMS |
|                     | 0.520   | 0.072              | 14                 | 0.540   | 0.035              | 7                  | 0.504  | 0.039              | 8                  | PTV |
| 4-Quadrants         | 0.108   | 0.009              | 9                  | 0.107   | 0.008              | 8                  | 0.114  | 0.022              | 21                 | RMS |
|                     | 0.519   | 0.079              | 15                 | 0.518   | 0.046              | 9                  | 0.542  | 0.080              | 16                 | PTV |
| Vortex (m=2)        | 0.101   | 0.004              | 4                  | 0.100   | 0.007              | 7                  | 0.110  | 0.006              | 5                  | RMS |
|                     | 0.502   | 0.042              | 8                  | 0.498   | 0.067              | 13                 | 0.531  | 0.040              | 8                  | PTV |

# Numerical results – Effect of Lyot stop

- Measurement accuracy is degraded by the Lyot stop
- WFE cannot be reconstructed if the diameters  $D$  and  $D_L$  of the telescope pupil and Lyot stop are equal
- Best measurement accuracy achieved when  $D_L / D \geq 3$

| $D_L/D$ ratio | Relative errors (%)            |     |                                  |     |
|---------------|--------------------------------|-----|----------------------------------|-----|
|               | Phase-shift in Lyot stop plane |     | Phase-shift in coronagraph plane |     |
|               | RMS                            | PTV | RMS                              | PTV |
| Negative      | 89                             | 85  | 85                               | 85  |
| 1             | Fail                           |     | Fail                             |     |
| 1.5           | 34                             | 23  | 37                               | 35  |
| 2             | 17                             | 16  | 20                               | 21  |
| 3             | 7                              | 13  | 10                               | 12  |
| 4             | 4                              | 12  | 6                                | 9   |
| 5             | 3                              | 12  | 5                                | 8   |
| 6             | 2                              | 11  | 5                                | 8   |
| 7             | 2                              | 11  | 5                                | 7   |
| 8             | 2                              | 11  | 4                                | 7   |



# Conclusion

- Phase-shifting techniques enable wavefront sensing behind the phase mask of a coronagraph
  - Potential reduction of Non common path aberration (NCPA)
- Phase-shifting can be implemented either in pupil or in image plane. In both cases measurement accuracy is well below  $\lambda/100$  RMS
  - This type of WFS is not limited to weak aberration, but only by  $2\pi$ -ambiguity
  - It not limited to low order spatial frequency (low order Zernike modes) and could operate in open loop
- Their performance is degraded when operating behind the Lyot stop
  - Optical solutions to be investigated: Independent optical arm ? “Dichroic” Lyot stop ? Integral field spectrograph ?

# Phase-shifting coronagraph is good !

- Questions ?